Modeling of Fault-tolerant Flux-switching Permanent-magnet Machines for Predicting Magnetic and Armature Reaction Fields

Ying Fang, Jinghua Ji, Wenxiang Zhao, *Senior Member, IEEE*

***Abstract*—The paper develops accurate analytical subdomain models for predicting the magnetic and armature reaction fields in fault-tolerant flux-switching permanent-magnet machines. The entire region is divided into five subdomains, followed by rotor slots, air-gap, stator slots, PM, and external air-gap imported to account for flux leakage. The coil turns and the remanence of magnets are adjusted by keeping the magnetic and electrical loading on the motor constant. The distance between the centers of two adjacent stator slots varies due to the introduction of fault-tolerant teeth. According to the variable separation method, the general solution expression of each region can be determined by solving the partial differential systems of equations. The magnetic field distributions of subdomains are obtained by applying the continuity conditions between adjacent regions. Some analytical field expressions are represented as new forms under armature reaction field condition compared to those under no-load condition. Based on the developed analytical models, the flux density distribution and the electromagnetic performance can be calculated under no-load or armature reaction field condition separately. The finite element analysis is carried out to verify the validity of the proposed analytical model.**

***Index Terms*—Armature reaction field, Fault-tolerant flux-switching machines, Magnetic field distribution, Permanent-magnet machine, Subdomain model.**

NOMENCLATURE

θ_0	Initial position of the rotor.
A_x	Vector potential in x domain.
θ_j	Position of the jth stator slot.
N_{st}	Stator slots number.
m	Harmonic order for rotor slots.
R_1	Internal radius of rotor slots.
R_2	External radius of rotor slots.
β_r	Rotor slots opening width.
θ_i	Position of the ith rotor slot.
n	Harmonic order for air-gap.
R_3	Internal radius of stator slots.
β_s	Stator slots opening width.
p	Harmonic order for stator slots.
R_4	External radius of stator slots.
β_f	PMs width.
θ_k	Position of the kth PM.
R_5	External radius of PMs.
q	Harmonic order for PMs.
t	Harmonic order for external air-gap.
B_{xr}	Radial flux density in x domain.
$B_{x\alpha}$	Tangential flux density in x domain.
N_c	Coil turns number.
A_c	Area of stator slot.
μ_0	Vacuum permeability.
μ_r	Relative magnetic permeability.
B_{rem}	Magnet remanence.
J_j	Current density in the jth stator slot.
Φ_1	Flux linkage of one slot.
l_{ef}	Axial length.
E	Phase back-electromotive force (EMF).
T	Torque.

Manuscript received February 10, 2022; revised March 08, 2022; accepted March 24, 2022. date of publication December 25, 2022; date of current version December 18, 2022.

This work was supported in part by the National Natural Science Foundation of China under Grants 51991383 and 52025073. *(Corresponding author: Jinghua Ji.)*

The authors are with the School of Electrical and Information Engineering, Jiangsu University, Zhenjiang 212013, China (e-mail: 2212007042@stmail.ujs.edu.cn; jjh@ujs.edu.cn; zwx@ujs.edu.cn;).

Digital Object Identifier 10.30941/CESTEMS.2022.00053

I. INTRODUCTION

In recent years, flux-switching permanent-magnet (FSPM) machines are attractive due to their simple rotor structure, high torque density and high reliability [1]−[3]. Besides, it is found that the introduction of fault-tolerant teeth (FTT) can bring about the merit of phase decoupling, thus improving the continued-operation capability. FT-FSPM machines have broad application prospects in the fields of aerospace and ship propulsions [4], [5]. However, the modeling and analysis of the FT-FSPM machine becomes difficult due to its double salient and FTT structure [6].

In general, the preliminary design and performance optimization of motors are modelled and analyzed by using numerical or analytical methods. The finite element analysis (FEA) is considered as the most effective numerical analysis method, which has the advantage of high accuracy [7]. FSPM machines are mostly studied by FEA and the general airgap field modulation theory in [8]−[10]. However, FEA is usually time-consuming and cannot correlate electromagnetic performances with structural parameters to provide guidance for optimization. Also, high mesh quality is required. In contrast, analytical methods consume less time and have

2096-3564 © 2022 CES

clearer physical principle. Some analytical methods have been proposed, including the separation variable method [11], the conformal mapping model [12]−[15], the magnetic equivalent circuit (MEC) method [16], relative permeance method [17], and subdomain model method [18]. In [11], the separation variable method was applied to brushless permanent magnet DC motors. Nevertheless, the magnetic field needs to have regular shape and homogeneous medium. In [12]−[15], the Schwarz-Christoffel mapping models were used for magnetic field analysis or performance optimization. The calculation processes were complex. Also, the models neglected the shape deformation of the magnets. In [16], the magnetic field of FT-FSPM machine was analytically calculated by the MEC method. The motor was equivalent to a magnetic network consisting of nonlinear magnetoresistance and flux sources according to the magnetic flux distribution. Although the MEC method can predict nonlinear magnetic field distribution, it has the disadvantage of complex calculations and the magnetic network structure varies with rotor position. In [17], a doubly-salient relative permeance method was presented to consider the slotting effect of the stator and rotor. The Cater factor and the complex relative permeance were adopted to compensate for the magnetic density with slotting considered. But the slotting effect on tangential flux density cannot be calculated accurately. In [18], general subdomain models for internal and external rotor multiphase FSPMMs were developed, and the subdomain model can also account for the slotting effect [19], [20]. Refs. [21]−[23] proposed subdomain models accounting for tooth-tips which are more suitable for motors with large slot opening and tooth top height. For the analytical methods, it already been proved that the subdomain model has excellent accuracy.

In this article, accurate analytical subdomain models will be developed to calculate the magnetic field of the FT-FSPM machine under no-load or armature reaction field condition, respectively. In addition, the fault-tolerant teeth and armature teeth are not equal in width. The positions of stator slots are redefined in the 2-D polar coordinate system. In Section II, the machine topology is illustrated and divided into several regions, viz. rotor slots, air-gap, stator slots, PM, and external air-gap. Some parameters of the motor are adjusted. In Section III, the general solution expression of each region is obtained by the variable separation method. Besides, the unknown coefficients are determined by applying the continuity conditions between adjacent subdomains. In Section IV, the analytical results are verified with FEA results. Finally, the conclusions are drawn in Section V.

II. Topology and Assumptions

A. Topology of FT-FSPM Machine

The cross-section of the 8/15-pole FT-FSPM machine is shown in Fig. 1. Both armature windings and PMs exist on the stator side, while PMs are held between the middle of the modular E-shaped laminated segments and tangentially magnetized in alternative opposite directions. The rotor adopts a simple salient pole structure and has 15 teeth. The FT-FSPM machine exhibits doubly salient structure and uses FTT to achieve the phase decoupling. Adjacent phase windings are inherently isolated. Therefore, its fault-tolerant performance is greatly improved. Due to the significant salient iron cores modulation effect, there are complex harmonic components in the air-gap field. Each phase winding consists of two coils in series, with a total of four phases. The application of concentrated windings can reduce copper loss.

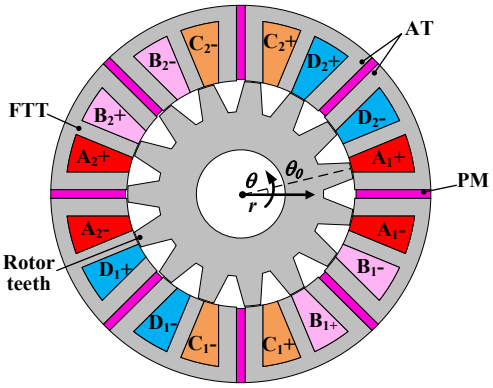

Fig. 1. Topology of 8/15-pole FT-FSPM machine.

The FT-FSPM machine is divided into five types of subdomains, followed by rotor slots, air-gap, stator slots, PM, and external air-gap imported to account for flux leakage. Each region is defined by its angular width and radial height in the 2-D polar coordinate system, as presented in Fig. 2.

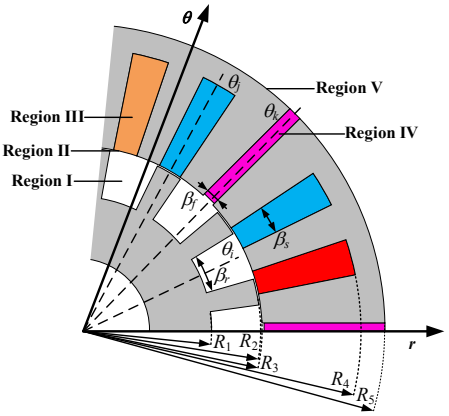

Fig. 2. Symbols and divisions in regions.

B. Main Assumptions and Adjustments

The following assumptions are made to facilitate the analysis:

1) Linear iron cores and demagnetization curve of PM.

2) The finite axial length is ignored, so the end effects are ruled out.

3) Stator/rotor laminations are non-conductive and isotropic.

4) Take no account of eddy current effect.

5) The current densities of slots are assumed to be uniform in the z-axis component.

It should be noted that the sides of each region are represented by components in the radial or angular direction. The adjusted geometry of the analytical model is displayed in Fig. 3, including rotor slots, PM and, stator slots. In order to keep the magnetic field modulation principle unaltered, the width of the rotor/stator teeth remains equal on the air-gap

side. Modifications to these regions will affect slots area and the effective volume of PMs. The remanence of the PMs should be adjusted by keeping the magnetic loading on the motor constant. The number of coil turns and the current density should be modified in order to obtain an equal slot fill rate and electrical loading. Some specific parameters before and after adjustment are compared in Table I.

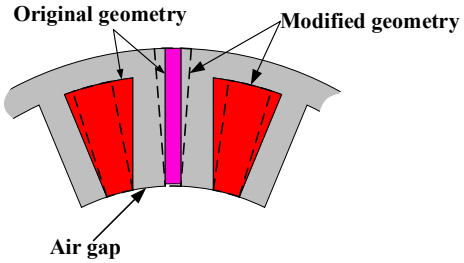

Fig. 3. Original and adjusted geometry.

TABLE I
COMPARISON OF SOME SPECIFIC PARAMETERS

Terms	FEA model	Subdomain model
Remanence of magnets (T)	1.4	1.2
Slots area (mm^2)	268.9	187.8
Number of coil turns	90	63
Phase current (A)	9	12.9

III. ANALYTICAL SUBDOMAIN MODELS

In this section, analytical subdomain models are developed in order to predict the open-circuit magnetic and armature reaction field distributions of the FT-FSPM machine, respectively. The magnetic field equations are given by solving the Laplace or Poisson equations. Besides, vector potential contains only z-axis component in 2-D field.

A. No-Load Subdomain Model

The flux density can be expressed by the magnetic field intensity and magnetization:

$$\mathbf{B} = \mu_0 \mu_r \mathbf{H} + \mu_0 \mathbf{M} \tag{1}$$

where μ_0 is the permeability of vacuum and μ_r is the relative permeability, respectively.

The PMs are magnetized along the tangential direction. The radial components of the magnetization vector of PMs are equal to zero. The tangential components can be described as

$$M_\theta = (-1)^{k-1} \frac{B_{rem}}{\mu_0},\ k = 1,\ 2,\ \cdots,\ N_{pm} \tag{2}$$

where B_{rem} is the remanence of magnets, N_{pm} is the number of PMs.

Due to the introduction of FTT, the representation of the slot center is more complicated. The widths of the fault-tolerant teeth and armature teeth are unequal. So, the positions of stator slots are defined as

$$\theta_j = \begin{cases} \theta_1 + \Delta_\theta \cdot \dfrac{(i-1)}{2},\ i = 1,\ 3,\ \cdots,\ N_{st}-1 \\ \theta_2 + \Delta_\theta \cdot (\dfrac{i}{2}-1),\ i = 2,\ 4,\ \cdots,\ N_{st} \end{cases} \tag{3}$$

where θ_j is the position of the center of the jth stator slot, θ_1 and θ_2 are the positions of the center of the 1th and 2th stator slot, N_{st} is the number of stator slots, $\Delta\theta$ is the span of the center of the adjacent odd or even slots.

The partial differential equations of each region are solved by the separation of variables method. The general solution applying boundary conditions between the slot bottom and iron core in rotor slots can be derived as

$$A_{1i}(r,\theta) = \sum_{m=1}^{\infty} A_{im}[(\frac{r}{R_2})^{\frac{m\pi}{\beta_r}} + (\frac{R_1}{R_2})^{\frac{m\pi}{\beta_r}} (\frac{r}{R_1})^{-\frac{m\pi}{\beta_r}}] \cdot \cos[\frac{m\pi}{\beta_r}(\theta + \frac{\beta_r}{2} - \theta_i)] \tag{4}$$

where R_1 is the internal radius of rotor slots, R_2 is the external radius of rotor slots, β_r is the rotor slot opening width, θ_i is the position of the center of the ith rotor slot, A_{im} is the unknown coefficient, m is the number of harmonics in rotor slots.

The general solution of the vector potential in the air-gap is

$$A_2(r,\theta) = \sum_{n=1}^{\infty}[B_{1n}(\frac{r}{R_3})^n + B_{2n}(\frac{r}{R_2})^{-n}]\cos(n\theta) + \sum_{n=1}^{\infty}[B_{3n}(\frac{r}{R_3})^n + B_{4n}(\frac{r}{R_2})^{-n}]\sin(n\theta) \tag{5}$$

where R_3 is the internal radius of stator slots, B_{1n}, B_{2n}, B_{3n}, and B_{4n} are the unknown coefficients, n is the number of harmonics in air-gap.

The general solution of the vector potential in stator slots can be given by

$$A_{3j}(r,\theta) = \sum_{p=1}^{\infty} C_{jp}[(\frac{R_4}{R_3})^{-\frac{p\pi}{\beta_s}} (\frac{r}{R_4})^{\frac{p\pi}{\beta_s}} + (\frac{r}{R_3})^{-\frac{p\pi}{\beta_s}}] \cdot \cos[\frac{p\pi}{\beta_s}(\theta + \frac{\beta_s}{2} - \theta_j)] + C_{j0} \tag{6}$$

where R_4 is the external radius of stator slots, β_s is the stator slot opening width, C_{jp} is the unknown coefficient, p is the number of harmonics in stator slots.

The governing function for the region of PMs is

$$\nabla^2 \mathbf{A} = -\mu_0 \nabla \times \mathbf{M} \tag{7}$$

$$\frac{\partial^2 A_{4k}}{\partial r^2} + \frac{1}{r}\frac{\partial A_{4k}}{\partial r} + \frac{1}{r^2}\frac{\partial^2 A_{4k}}{\partial \theta^2} = -\frac{\mu_0}{r} M_\theta \tag{8}$$

the general solution of the vector potential in PMs can be expressed by

$$A_{4k}(r,\theta) = \sum_{q=1}^{\infty}[D_{k1q}(\frac{r}{R_5})^{\frac{q\pi}{\beta_f}} + D_{k2q}(\frac{r}{R_3})^{-\frac{q\pi}{\beta_f}}] \cdot \cos[\frac{q\pi}{\beta_f}(\theta + \frac{\beta_f}{2} - \theta_k)] - (-1)^{k-1} B_{rem} \cdot r + D_{k10} + D_{k20} \ln r \tag{9}$$

where R_5 is the external radius of PMs, β_f is the PM width, θ_k is the position of the center of the kth PM, D_{k1q}, D_{k2q}, D_{k10}, and D_{k20} are the unknown coefficients, q is the number of harmonics in PMs.

The radius of the external air-gap is thought to extend to infinity. Since the flux linkage is closed, the vector potential at infinity is equal to zero. The general solution in external air-gap can be given by

$$A_5(r,\theta)=\sum_{t=1}^{\infty}F_{1t}[(\frac{r}{R_5})^{-t}]\cos(t\theta)+\sum_{t=1}^{\infty}F_{2t}[(\frac{r}{R_5})^{-t}]\sin(t\theta) \quad (10)$$

where F_{1t}, F_{2t} are the unknown coefficients, t is the number of harmonics in the external air-gap.

The radial and circumferential components of flux density can be calculated by

$$B_r=\frac{1}{r}\frac{\partial A_z}{\partial \alpha} \quad (11)$$

$$B_\alpha=-\frac{\partial A_z}{\partial r} \quad (12)$$

The expressions of flux densities in each subdomain can be obtained:

$$B_{1ir}=-\sum_{m=1}^{\infty}E_1A_{im}[\frac{1}{R_2}(\frac{r}{R_2})^{E_1-1}+\frac{G_1}{R_1}(\frac{r}{R_1})^{-E_1-1}]\cdot\sin[E_1(\theta+\frac{\beta_r}{2}-\theta_i)] \quad (13)$$

$$B_{1i\alpha}=-\sum_{m=1}^{\infty}E_1A_{im}[\frac{1}{R_2}(\frac{r}{R_2})^{E_1-1}-\frac{G_1}{R_1}(\frac{r}{R_1})^{-E_1-1}]\cdot\cos[E_1(\theta+\frac{\beta_r}{2}-\theta_i)] \quad (14)$$

and

$$E_1=\frac{m\pi}{\beta_r} \quad (15)$$

$$G_1=(\frac{R_1}{R_2})^{\frac{m\pi}{\beta_r}} \quad (16)$$

in air-gap,

$$B_{2r}=-\sum_{n=1}^{\infty}n[\frac{B_{1n}}{R_3}(\frac{r}{R_3})^{n-1}+\frac{B_{2n}}{R_2}(\frac{r}{R_2})^{-n-1}]\sin(n\theta)+\sum_{n=1}^{\infty}n[\frac{B_{3n}}{R_3}(\frac{r}{R_3})^{n-1}+\frac{B_{4n}}{R_2}(\frac{r}{R_2})^{-n-1}]\cos(n\theta) \quad (17)$$

$$B_{2\alpha}=-\sum_{n=1}^{\infty}n[\frac{B_{1n}}{R_3}(\frac{r}{R_3})^{n-1}-\frac{B_{2n}}{R_2}(\frac{r}{R_2})^{-n-1}]\cos(n\theta)-\sum_{n=1}^{\infty}n[\frac{B_{3n}}{R_3}(\frac{r}{R_3})^{n-1}-\frac{B_{4n}}{R_2}(\frac{r}{R_2})^{-n-1}]\sin(n\theta) \quad (18)$$

in stator slots,

$$B_{3jr}=-\sum_{p=1}^{\infty}E_2C_{jp}[\frac{G_3}{R_4}(\frac{r}{R_4})^{E_2-1}+\frac{1}{R_3}(\frac{r}{R_3})^{-E_2-1}]\cdot\sin[E_2(\theta+\frac{\beta_s}{2}-\theta_j)] \quad (19)$$

$$B_{3j\alpha}=-\sum_{p=1}^{\infty}E_2C_{jp}[\frac{G_3}{R_4}(\frac{r}{R_4})^{E_2-1}-\frac{1}{R_3}(\frac{r}{R_3})^{-E_2-1}]\cdot\cos[E_2(\theta+\frac{\beta_s}{2}-\theta_j)] \quad (20)$$

and

$$E_2=\frac{p\pi}{\beta_s} \quad (21)$$

$$G_3=(\frac{R_3}{R_4})^{\frac{p\pi}{\beta_s}} \quad (22)$$

in PMs,

$$B_{4kr}=-\sum_{q=1}^{\infty}E_3[\frac{D_{k1q}}{R_5}(\frac{r}{R_5})^{E_3-1}+\frac{D_{k2q}}{R_3}(\frac{r}{R_3})^{-E_3-1}]\cdot\sin[E_3(\theta+\frac{\beta_f}{2}-\theta_k)] \quad (23)$$

$$B_{4k\alpha}=-\sum_{q=1}^{\infty}E_3[\frac{D_{k1q}}{R_5}(\frac{r}{R_5})^{E_3-1}-\frac{D_{k2q}}{R_3}(\frac{r}{R_3})^{-E_3-1}]\cdot\cos[\frac{q\pi}{\beta_f}(\theta+\frac{\beta_f}{2}-\theta_k)]+(-1)^{k-1}B_{rem}-\frac{D_{k20}}{r} \quad (24)$$

in external air-gap,

$$B_{5r}=-\sum_{t=1}^{\infty}t[\frac{F_{1t}}{R_5}(\frac{r}{R_5})^{-t-1}]\sin(t\theta)+\sum_{t=1}^{\infty}t[\frac{F_{2t}}{R_5}(\frac{r}{R_5})^{-t-1}]\cos(t\theta) \quad (25)$$

$$B_{5\alpha}=-\sum_{t=1}^{\infty}t[-\frac{F_{1t}}{R_5}(\frac{r}{R_5})^{-t-1}]\cos(t\theta)-\sum_{t=1}^{\infty}t[-\frac{F_{2t}}{R_5}(\frac{r}{R_5})^{-t-1}]\sin(t\theta) \quad (26)$$

obviously, there are various unknown coefficients in the above general solutions from (4) to (10) to be determined. Therefore, the interface conditions based on the continuity of the vector potential or magnetic field intensity between contiguous regions should be considered.

For rotor slots and air-gap, the vector potential and circumferential magnetic field intensity is continuous at the slot opening:

$$A_{1i}\Big|_{r=R_2}=A_2\Big|_{r=R_2} \quad (27)$$

$$H_{1\theta}\Big|_{r=R_2}=H_{2\theta}\Big|_{r=R_2} \quad (28)$$

for air-gap and stator slots/PMs, the boundary conditions can be expressed as

$$A_2\Big|_{r=R_3}=A_{3j}\Big|_{r=R_3} \quad (29)$$

$$A_2\Big|_{r=R_3}=A_{4k}\Big|_{r=R_3} \quad (30)$$

$$H_{2\theta}\Big|_{r=R_3}=\begin{cases}H_{3j\theta}\Big|_{r=R_3}, -\frac{\beta_s}{2}+\theta_j\le\theta\le\frac{\beta_s}{2}+\theta_j\\ \frac{1}{\mu_r}(H_{4k\theta}\Big|_{r=R_3}+(-1)^{k-1}B_{rem})\\ \quad -\frac{\beta_f}{2}+\theta_k\le\theta\le\frac{\beta_f}{2}+\theta_k\\ 0, elsewhere\end{cases} \quad (31)$$

for PMs and external air-gap, the interface conditions can be expressed as

$$A_5\Big|_{r=R_5}=A_{4k}\Big|_{r=R_5} \quad (32)$$

$$H_{5\theta}\Big|_{r=R_5}=\frac{1}{\mu_r}H_{4k\theta}\Big|_{r=R_5} \quad (33)$$

When applying these interface conditions, different subdomains have respective distribution intervals which

should be unified by the Fourier series expansion. The Fourier analysis process is given in the Appendix. Equs. (46)−(56) can be written in the matrix format. The unknown coefficients can be determined to calculate the magnetic field distribution.

B. Armature Reaction Field Subdomain Model

The vector potential in stator slots satisfies the following governing functions:

$$\nabla^2 \times \mathbf{A} = -\mu_0 \mathbf{J} \tag{34}$$

$$\frac{\partial^2 A_{3j}}{\partial r^2} + \frac{1}{r}\frac{\partial A_{3j}}{\partial r} + \frac{1}{r^2}\frac{\partial^2 A_{3j}}{\partial \theta^2} = -\mu_0 J \tag{35}$$

where **J** is the current density.

The current density in the stator slots with single-layer concentrated winding as shown in Fig.4, can be expressed as:

$$\mathbf{J_j} = \frac{N_c \mathbf{C_j}}{A_c}\begin{bmatrix} i_a & i_b & i_c & i_d \end{bmatrix} \tag{36}$$

where $\mathbf{J_j}$ represents the current density matrix in the stator slots, N_c is the number of coil turns, A_c is the slot coil area, $\mathbf{C_j}$ is the distribution matrix of armature windings.

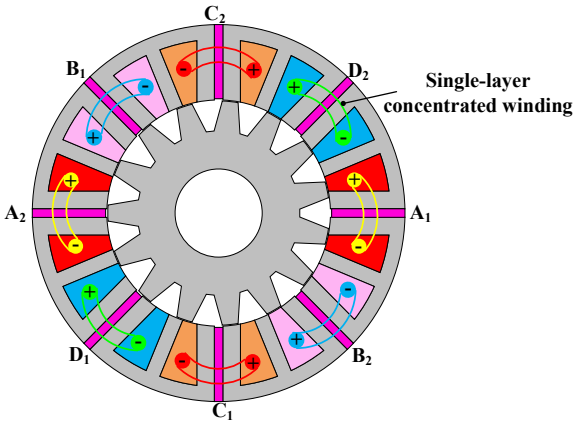

Fig. 4. Current density distribution.

The general solution of the vector potential in stator slots can be given by

$$A_{3j}(r,\theta) = \sum_{p=1}^{\infty} C_{jp}\left[\left(\frac{R_4}{R_3}\right)^{-\frac{p\pi}{\beta_s}}\left(\frac{r}{R_4}\right)^{\frac{p\pi}{\beta_s}} + \left(\frac{r}{R_3}\right)^{-\frac{p\pi}{\beta_s}}\right] \cdot\cos\left[\frac{p\pi}{\beta_s}\left(\theta + \frac{\beta_s}{2} - \theta_j\right)\right] + \frac{1}{2}\mu_0 J_j R_4^{\,2}\ln r - \frac{1}{4}\mu_0 J_j r^2 + C_{j0} \tag{37}$$

where C_{jp}, C_{j0} are the unknown coefficients.

The expressions of general solutions for the rotor slots, air-gap, and external air-gap subdomains are the same as under no-load condition, while in PMs, the formula becomes:

$$A_{4k}(r,\theta) = \sum_{q=1}^{\infty}\left[D_{k1q}\left(\frac{r}{R_5}\right)^{\frac{q\pi}{\beta_f}} + D_{k2q}\left(\frac{r}{R_3}\right)^{-\frac{q\pi}{\beta_f}}\right] \cdot\cos\left[\frac{q\pi}{\beta_f}\left(\theta + \frac{\beta_f}{2} - \theta_k\right)\right] \tag{38}$$

correspondingly, the flux densities of armature reaction field can be calculated in stator slots,

$$B_{3jr}(r,\theta) = -\sum_{p=1}^{\infty} E_2 C_{jp}\left[\frac{G_3}{R_4}\left(\frac{r}{R_4}\right)^{E_2-1} + \frac{1}{R_3}\left(\frac{r}{R_3}\right)^{-E_2-1}\right]\cdot\sin\left[E_2\left(\theta + \frac{\beta_s}{2} - \theta_j\right)\right] \tag{39}$$

$$B_{3j\alpha} = -\sum_{p=1}^{\infty} E_2 C_{jp}\left[\frac{G_3}{R_4}\left(\frac{r}{R_4}\right)^{E_2-1} - \frac{1}{R_3}\left(\frac{r}{R_3}\right)^{-E_2-1}\right] \cdot\cos\left[E_2\left(\theta + \frac{\beta_s}{2} - \theta_j\right)\right] - \frac{1}{2}\mu_0 J_j R_4^{\,2}/r + \frac{1}{2}\mu_0 J_j r \tag{40}$$

in PMs,

$$B_{4kr} = -\sum_{q=1}^{\infty} E_3\left[\frac{D_{k1q}}{R_5}\left(\frac{r}{R_5}\right)^{E_3-1} + \frac{D_{k2q}}{R_3}\left(\frac{r}{R_3}\right)^{-E_3-1}\right] \cdot\sin\left[E_3\left(\theta + \frac{\beta_f}{2} - \theta_k\right)\right] \tag{41}$$

$$B_{4k\alpha} = -\sum_{q=1}^{\infty} E_3\left[\frac{D_{k1q}}{R_5}\left(\frac{r}{R_5}\right)^{E_3-1} - \frac{D_{k2q}}{R_3}\left(\frac{r}{R_3}\right)^{-E_3-1}\right] \cdot\cos\left[E_3\left(\theta + \frac{\beta_f}{2} - \theta_k\right)\right] \tag{42}$$

Applying the same boundary conditions from (27) to (33), the appropriate harmonic order for each region can lead to more accurate analytical results.

IV. Verification

In this section, the analytical results are compared with solutions obtained by 2-D linear FEA to evaluate the accuracy of analytical method. The parameters of the 8/15-pole FT-FSPM machine are listed in Table II.

TABLE II
Parameters of FT-FSPM Machine

Types	8/15-pole
Rated power (kW)	1.2
Rated torque (Nm)	24
Stator outside diameter (mm)	154
Stator inside diameter (mm)	92.4
Rotor inside diameter (mm)	36
Air-gap length (mm)	0.4
Axial length (mm)	60
Stator tooth arc (degree)	7.06
FTT arc (degree)	6.16
Rotor tooth arc (degree)	6.7
Number of coil turns	90
Slot packing factor	0.5

Figs. 5 and 7 compare the radial and tangential components of the air-gap flux density between FEA and subdomain model under no-load or armature reaction field condition, respectively. The radius is chosen in the center of the air-gap. It can be observed that the solutions show good agreement between subdomain model and FEA.

Figs. 6 and 8 compare the harmonics in air-gap radial flux density predicted by FEA and subdomain model in two cases. The error of each harmonic amplitude between analytical results and FEA results does not exceed 0.15T. The proposed subdomain model is also verified to have high consistency with FEA from the perspective of harmonic analysis.

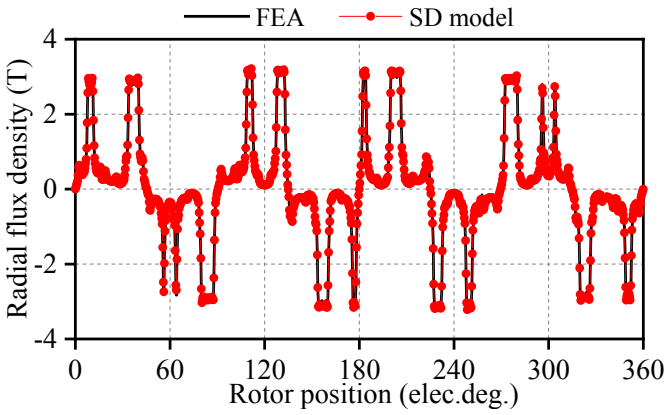

(a)

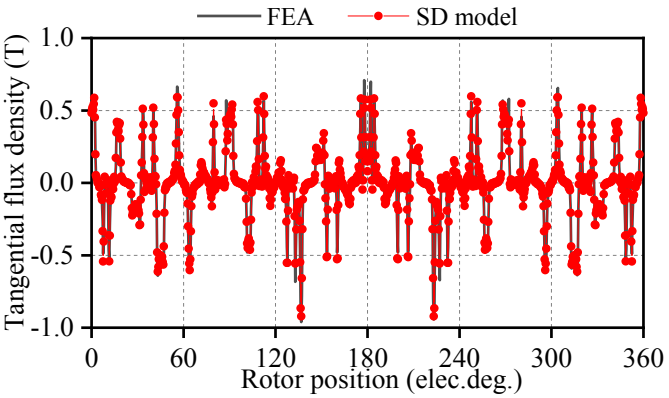

(b)

Fig. 5. Air-gap flux density under no-load condition. (a) Radial component. (b) Tangential component.

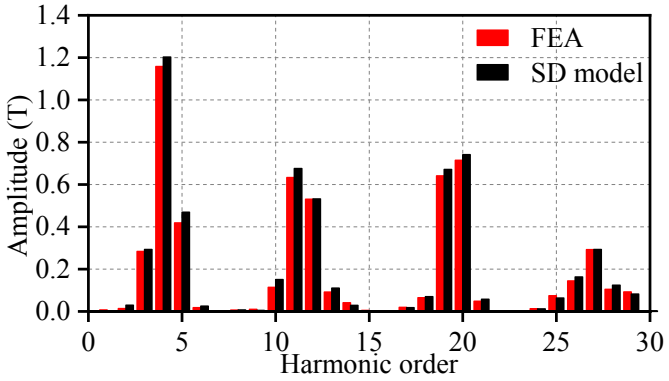

Fig. 6. Harmonics in air-gap radial flux density under no-load condition.

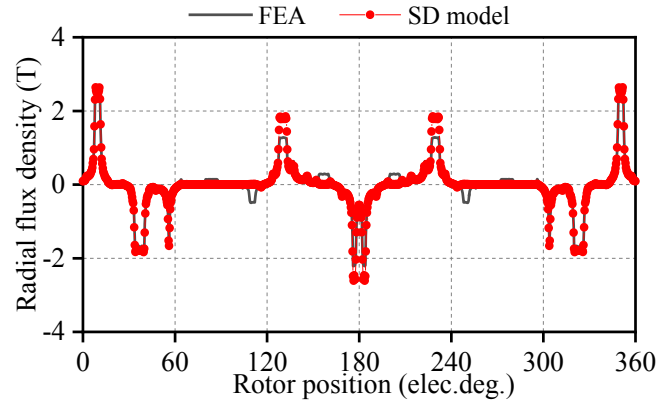

(a)

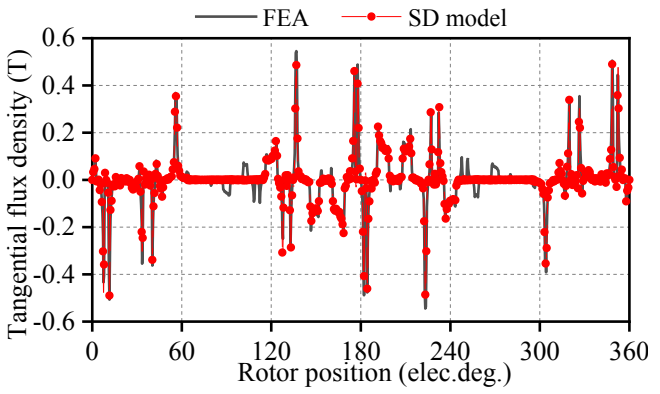

(b)

Fig. 7. Air-gap flux density under armature reaction field condition. (a) Radial component. (b) Tangential component.

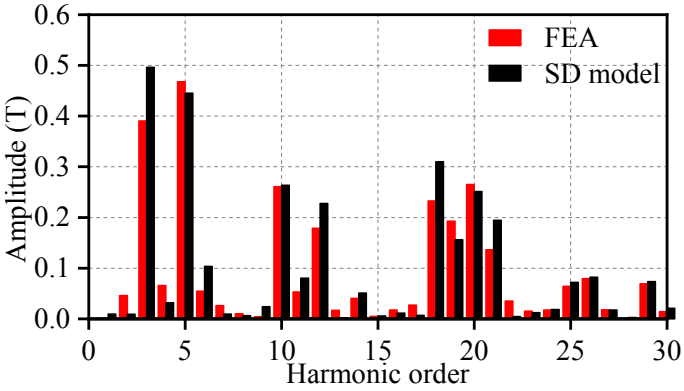

Fig. 8. Harmonics in air-gap radial flux density under armature reaction field condition.

The flux linkage of one slot can be calculated from the vector potential in the stator slot

$$\Phi_1 = l_{ef}\frac{N_c}{A_c}\int_{R_3}^{R_4}\int_{\theta_j-\frac{\beta_s}{2}}^{\theta_j+\frac{\beta_s}{2}} A_{3j}\,r dr d\theta \tag{43}$$

where l_{ef} is the axial length, N_c is the coil turns, A_c is the area of one slot. The flux linkage of one phase is the sum of the flux linkages of the total slots corresponding to the phase. Then, the back-EMF is calculated by the flux linkage

$$E = -\frac{d\Phi}{dt} \tag{44}$$

Figs. 9 and 10 compare the flux linkage and back-EMF of one phase. The results show good agreement between analytical model and FEA.

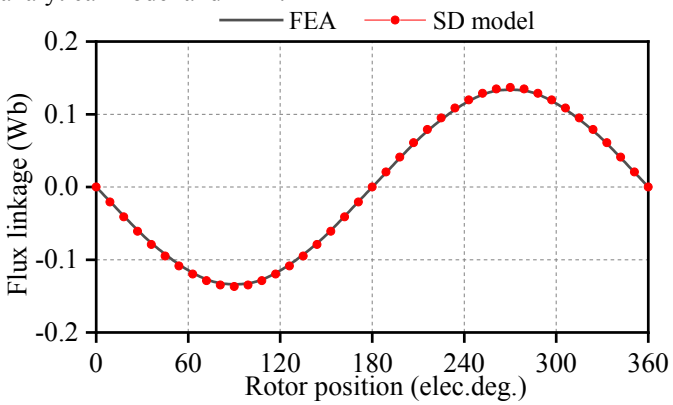

Fig. 9. Flux linkage of A phase.

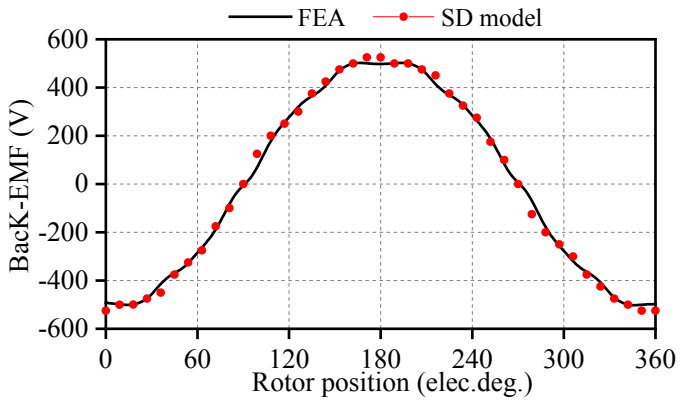

Fig. 10. Phase back-EMF.

The cogging torque and the output torque can be calculated by applying Maxwell stress tensor method

$$T = \frac{l_{ef} r^2}{\mu_0} \int_0^{2\pi} B_{2r} B_{2\theta} d\theta \tag{45}$$

Figs. 11 and 12 compare the cogging torque and electromagnetic torque. The results between FEA and analytical model are very close. Therefore, the subdomain model can be used for the calculation of the electromagnetic performance.

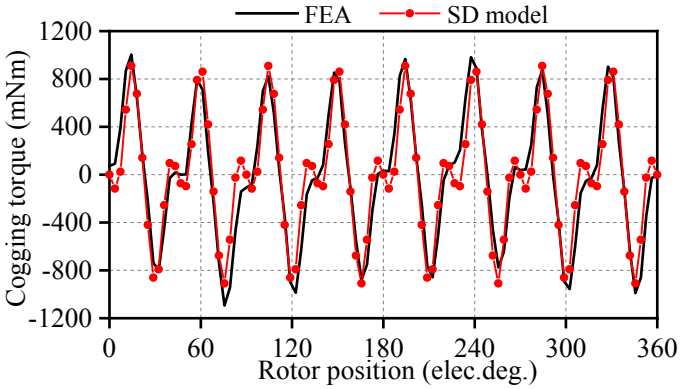

Fig. 11. Cogging torque.

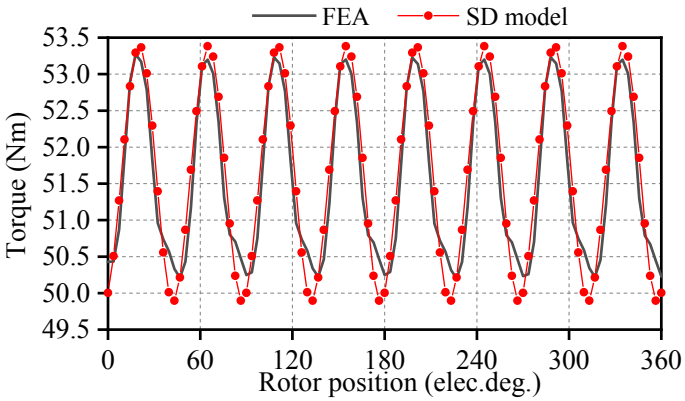

Fig. 12. Electromagnetic torque.

V. Conclusion

This paper has newly developed accurate subdomain models to predict the magnetic and armature reaction fields in the 8/15-pole FT-FSPM machine. The entire domain is divided into five regions and the width and angle definitions used in the analytical model are marked. The coil turns and the remanence of PMs are adjusted to offset the effect of modifications in geometry parameters. The positions of stator slots are redefined due to the FTT. The expressions of magnetic field distributions in two cases are obtained according to boundary conditions and the interface conditions. Then the flux densities of each subdomain are calculated according to the relationship between the magnetic field and the vector potential. The proposed analytical subdomain models have a high accuracy in predicting both air-gap flux density and harmonic compositions. It is also valuable to predict other electromagnetic performances, such as the cogging torque and the output torque, back-EMF and eddy-current losses in magnets. The model can also be a guidance for the preliminary design and performance optimization of FT-FSPM machines.

Appendix

According to the interface conditions above from (27) to (33), the Fourier transform process under no-load conditions is presented below. From (27), it can be obtained:

$$\begin{aligned} A_i[1+G_1^2] = &\sum_{n=1}^{\infty} B_1 G_2 \cdot \sigma_i(m,n) + \sum_{n=1}^{\infty} B_2 \cdot \sigma_i(m,n) \\ &+ \sum_{n=1}^{\infty} B_3 G_2 \cdot \lambda_i(m,n) + \sum_{n=1}^{\infty} B_4 \cdot \lambda_i(m,n) \end{aligned} \tag{46}$$

and

$$\sigma_i(m,n) = \frac{2}{\beta_r} \frac{n}{n^2 - E_1^2} (\cos(m\pi)\sin(n\frac{\beta_r}{2} + n\theta_i) - \sin(n\theta_i - n\frac{\beta_r}{2}))$$

$$\lambda_i(m,n) = \frac{-2}{\beta_r} \frac{n}{n^2 - E_1^2} (\cos(m\pi)\cos(n\frac{\beta_r}{2} + n\theta_i) - \cos(n\theta_i - n\frac{\beta_r}{2}))$$

$$E_1 = \frac{m\pi}{\beta_r},\ G_1 = (\frac{R_1}{R_2})^{\frac{m\pi}{\beta_r}},\ G_2 = (\frac{R_2}{R_3})^n$$

from (28), it can be obtained:

$$[B_{1n} G_2 - B_{2n}] = \sum_{i=1}^{N_r} \sum_{m=1}^{\infty} A_{im} [1 - G_1^2] K_i(m,n) \tag{47}$$

$$[B_{3n} G_2 - B_{4n}] = \sum_{i=1}^{N_r} \sum_{m=1}^{\infty} A_{im} [1 - G_1^2] S_i(m,n) \tag{48}$$

and

$$K_i(m,n) = \frac{m}{\beta_r} \frac{1}{n^2 - E_1^2} [\cos(m\pi)\sin(n\theta_i + \frac{n\beta_r}{2}) - \sin(n\theta_i - \frac{n\beta_r}{2})]$$

$$S_i(m,n) = \frac{-m}{\beta_r} \frac{1}{n^2 - E_1^2} [\cos(m\pi)\cos(n\theta_i + \frac{n\beta_r}{2}) - \cos(n\theta_i - \frac{n\beta_r}{2})]$$

from (29), it can be obtained:

$$\begin{aligned} C_{jp}[G_3^2 + 1] = &\sum_{n=1}^{\infty} [B_{1n} + B_{2n} G_2] \omega_j(p,n) \\ &+ \sum_{n=1}^{\infty} [B_{3n} + B_{4n} G_2] \psi_j(p,n) \end{aligned} \tag{49}$$

and

$$\omega_j(p,n) = \frac{2}{\beta_s} \frac{n}{n^2 - E_2^2} [\cos(p\pi)\sin(n\theta_j + \frac{n\beta_s}{2}) - \sin(n\theta_j - \frac{n\beta_s}{2})]$$

$$\psi_j(p,n)=-\frac{2}{\beta_s}\frac{n}{n^2-E_2^{\,2}}[\cos(p\pi)\cos(n\theta_j+\frac{n\beta_s}{2})-\cos(n\theta_j-\frac{n\beta_s}{2})]$$

$$E_2=\frac{p\pi}{\beta_s},\ G_2=(\frac{R_2}{R_3})^n,\ G_3=(\frac{R_3}{R_4})^{\frac{p\pi}{\beta_s}}$$

from (30), it can be obtained:

$$\begin{aligned}&-(-1)^{k-1}B_{rem}R_3+D_{k10}+D_{k20}\ln R_3=\\&\sum_{n=1}^{\infty}[B_{1n}+B_{2n}G_2]P_k(n)+\sum_{n=1}^{\infty}[B_{3n}+B_{4n}G_2]Q_k(n)\end{aligned}\tag{50}$$

$$\begin{aligned}D_{k1}G_4+D_{k2}&=\sum_{\mathrm{n}=1}^{\infty}[B_{1n}+B_{2n}G_2]X_k(q,n)\\&+\sum_{n=1}^{\infty}[B_{3n}+B_{4n}G_2]Y_k(q,n)\end{aligned}\tag{51}$$

and

$$P_k(n)=\frac{1}{n\beta_f}(\sin(n\frac{\beta_f}{2}+n\theta_k)-\sin(n\theta_k-n\frac{\beta_f}{2}))$$

$$Q_k(n)=\frac{-1}{n\beta_f}(\cos(n\frac{\beta_f}{2}+n\theta_k)-\cos(n\theta_k-n\frac{\beta_f}{2}))$$

$$X_k(q,n)=\frac{2}{\beta_f}\frac{n}{n^2-E_3^{\,2}}[\cos(q\pi)\sin(n\theta_k+\frac{n\beta_f}{2})-\sin(n\theta_k-\frac{n\beta_f}{2})]$$

$$Y_k(q,n)=-\frac{2}{\beta_f}\frac{n}{n^2-E_3^{\,2}}[\cos(q\pi)\cos(n\theta_k+\frac{n\beta_f}{2})-\cos(n\theta_k-\frac{n\beta_f}{2})]$$

$$E_3=\frac{q\pi}{\beta_f},\ G_2=(\frac{R_2}{R_3})^n,\ G_4=(\frac{R_3}{R_5})^{\frac{q\pi}{\beta_f}}$$

from (31), it can be obtained:

$$\begin{aligned}[B_{1n}-B_{2n}G_2]&=\sum_{j=1}^{N_s}\sum_{p=1}^{\infty}C_{jp}[G_3^{\,2}-1]A_j(p,n)+\\&\sum_{k=1}^{N_{pm}}\sum_{q=1}^{\infty}[D_{k1}G_4-D_{k2}]B_k(q,n)+\sum_{k=1}^{N_{pm}}\frac{D_{k20}}{R_3}C_k(n)\end{aligned}\tag{52}$$

$$\begin{aligned}[B_{3n}-B_{4n}G_2]&=\sum_{j=1}^{N_s}\sum_{p=1}^{\infty}C_{jp}[G_3^{\,2}-1]D_j(p,n)+\\&+\sum_{k=1}^{N_{pm}}\sum_{q=1}^{\infty}[D_{k1}G_4-D_{k2}]\cdot E_k(q,n)\\&+\sum_{k=1}^{N_{pm}}(-K_kB_{rem})F_k(n)+\sum_{k=1}^{N_{pm}}\frac{D_{k20}}{R_3}F_k(n)\end{aligned}\tag{53}$$

and

$$A_j(p,n)=\frac{p}{\beta_s}\frac{1}{n^2-E_2^{\,2}}[\cos(p\pi)\sin(n\theta_j+\frac{n\beta_s}{2})-\sin(n\theta_j-\frac{n\beta_s}{2})]$$

$$B_k(q,n)=\frac{q}{\beta_f\mu_r}\frac{1}{n^2-E_3^{\,2}}[\cos(q\pi)\sin(n\theta_k+\frac{n\beta_f}{2})-\sin(n\theta_k-\frac{n\beta_f}{2})]$$

$$C_k(n)=\frac{R_3}{n^2\pi\mu_r}[\sin(n\theta_k+\frac{n\beta_f}{2})-\sin(n\theta_k-\frac{n\beta_f}{2})]$$

$$D_j(p,n)=\frac{-p}{\beta_s}\frac{1}{n^2-E_2^{\,2}}[\cos(p\pi)\cos(n\theta_j+\frac{n\beta_s}{2})-\cos(n\theta_j-\frac{n\beta_s}{2})]$$

$$E_k(q,n)=\frac{-q}{\beta_f\mu_r}\frac{1}{n^2-E_3^{\,2}}[\cos(q\pi)\cos(n\theta_k+\frac{n\beta_f}{2})-\cos(n\theta_k-\frac{n\beta_f}{2})]$$

$$F_k(n)=\frac{-R_3}{n^2\pi\mu_r}[\cos(n\theta_k+\frac{n\beta_f}{2})-\cos(n\theta_k-\frac{n\beta_f}{2})]$$

from (32), it can be obtained:

$$\begin{aligned}&-(-1)^{k-1}B_{rem}R_5+D_{k10}\\&+D_{k20}\ln R_5=\sum_{t=1}^{\infty}F_{1t}M_k(t)+\sum_{t=1}^{\infty}F_{2t}N_k(t)\end{aligned}\tag{54}$$

$$D_{k1}+D_{k2}G_4=\sum_{t=1}^{\infty}F_{1t}H_k(q,t)+\sum_{t=1}^{\infty}F_{2t}I_k(q,t)\tag{55}$$

and

$$M_k(t)=\frac{1}{t\beta_f}(\sin(t\frac{\beta_f}{2}+t\theta_k)-\sin(t\theta_k-t\frac{\beta_f}{2}))$$

$$N_k(t)=\frac{-1}{t\beta_f}(\cos(t\frac{\beta_f}{2}+t\theta_k)-\cos(t\theta_k-t\frac{\beta_f}{2}))$$

$$H_k(q,t)=\frac{2}{\beta_f}\frac{t}{t^2-E_3^{\,2}}[\cos(q\pi)\sin(t\theta_k+\frac{t\beta_f}{2})-\sin(t\theta_k-\frac{t\beta_f}{2})]$$

$$I_k(q,t)=-\frac{2}{\beta_f}\frac{t}{t^2-E_3^{\,2}}[\cos(q\pi)\cos(t\theta_k+\frac{t\beta_f}{2})-\cos(t\theta_k-\frac{t\beta_f}{2})]$$

from (33), it can be obtained:

$$\begin{aligned}-F_{1t}&=\sum_{k=1}^{N_{pm}}\sum_{q=1}^{\infty}[D_{k1q}-D_{k2q}G_4]G_{\mathrm{k}}(q,t)\\&+\sum_{k=1}^{N_{pm}}(-K_KB_{rem})J_k(t)+\sum_{k=1}^{N_{pm}}(D_{k20}/R_5)J_k(t)\end{aligned}\tag{56}$$

and

$$G_k(q,t)=\frac{q}{\mu_r\beta_f}\frac{1}{t^2-E_3^{\,2}}[\cos(q\pi)\sin(t\theta_k+\frac{t\beta_f}{2})-\sin(t\theta_k-\frac{t\beta_f}{2})]$$

$$J_k(t)=\frac{R_5}{\mu_rt^2\pi}[\sin(t\theta_k+\frac{t\beta_f}{2})-\sin(t\theta_k-\frac{t\beta_f}{2})]$$

$$R_k(q,t)=\frac{-q}{\mu_r\beta_f}\frac{1}{t^2-E_3^{\,2}}[\cos(q\pi)\cos(t\theta_k+\frac{t\beta_f}{2})-\cos(t\theta_k-\frac{t\beta_f}{2})]$$

$$L_k(t)=\frac{-R_5}{\mu_rt^2\pi}[\cos(t\theta_k+\frac{t\beta_f}{2})-\cos(t\theta_k-\frac{t\beta_f}{2})]$$

$$E_3=\frac{q\pi}{\beta_f},\ G_5=-(\frac{R_5}{R_6})^{2t},\ G_4=(\frac{R_3}{R_5})^{\frac{q\pi}{\beta_f}}$$

REFERENCES

[1] W. Zhao, X. Pan, J. Ji, L. Xu, and J. Zheng, "Analysis of PM eddy current loss in four-phase fault-tolerant flux-switching permanent-magnet machines by air-gap magnetic field modulation theory," *IEEE Trans. Ind. Electron.*, vol. 67, no. 7, pp. 5369−5378, Jul. 2020.

[2] W. Li and M. Cheng, "Reliability analysis and evaluation for flux-switching permanent magnet machine," *IEEE Trans. Ind. Electron.*, vol. 66, no. 3, pp. 1760−1769, Mar. 2019.

[3] X. Zhu, W. Hua, Z. Wu, W. Huang, H. Zhang, and M. Cheng, "Analytical approach for cogging torque reduction in flux-switching permanent magnet machines based on magnetomotive force-permeance model," *IEEE Trans. Ind. Electron.*, vol. 65, no. 3, pp. 1965−1979, Mar. 2018.

[4] J. Luo *et al.*, "Reduction of eddy-current loss in flux-switching permanent-magnet machines using rotor magnetic flux barriers," *IEEE Trans. Magn.*, vol. 53, no. 11, Nov. 2017, Art no. 2300605.

[5] L. Wu, J. Zhu, and Y. Fang, "A novel doubly-fed flux-switching permanent magnet machine with armature windings wound on both stator poles and rotor teeth," *IEEE Trans. Ind. Electron.,* vol. 67, no. 12, pp. 10223−10232, Dec. 2020.

[6] B. L. J. Gysen, E. Ilhan, K. J. Meessen, J. J. H. Paulides, and E. A. Lomonova, "Modeling of flux switching permanent magnet machines with Fourier analysis," *IEEE Trans. Magn.*, vol. 46, no. 6, pp. 1499−1502, Jun. 2010.

[7] I. C. Vese, F. Marignetti, and M. M. Radulescu, "Multiphysics approach to numerical modeling of a permanent-magnet tubular linear motor," *IEEE Trans. Ind. Electron.*, vol. 57, no. 1, pp. 320−326, Jan. 2010.

[8] J. Wang, M. Cheng, W. Tian, and Y. Jiang, "Iron loss calculation for FSPM machine with the PWM inverter supply based on general airgap field modulation theory," *IEEE Trans. Ind. Electron.,* DOI: 10.1109/TIE.2021.3135615.

[9] P. Su, W. Hua, M. Hu, Z. Chen, M. Cheng, and W. Wang, "Analysis of PM eddy current loss in rotor-PM and stator-PM flux-switching machines by air-gap field modulation theory," *IEEE Trans. Ind. Electron.*, vol. 67, no. 3, pp. 1824−1835, Mar. 2020.

[10] P. Wang, W. Hua, G. Zhang, B. Wang, and M. Cheng, "Inductance characteristics of flux-switching permanent magnet machine based on general air-gap filed modulation theory," *IEEE Trans. Ind. Electron.*, DOI: 10.1109/TIE.2021.3130334.

[11] Z. Q. Zhu, D. Howe, E. Bolte, and B. Ackermann, "Instantaneous magnetic field distribution in brushless permanent magnet DC motors. I. Open-circuit field," *IEEE Trans. Magn.*, vol. 29, no. 1, pp. 124−135, Jan. 1993.

[12] Open-circuit field," *IEEE Trans. Magn.*, vol. 29, no. 1, pp. 124−135, Jan. 1993.

[13] Z. Ding, X. Wu, and C. Chen, "Analytical calculation of no-load air gap magnetic field of surface mounted permanent magnet motor based on Schwarz-Christoffel transformation," in *Proc. IEEE Int. Conf. Elect. Mach. Syst.*, Gyeongju, Korea, Dec. 2021, pp. 1085−1089.

[14] N. Chiodetto, N. Bianchi, and L. Alberti, "Improved analytical estimation of rotor losses in high-speed surface-mounted PM synchronous machines," *IEEE Trans. Ind. Appl.*, vol. 53, no. 4, pp. 3548−3556, Aug. 2017.

[15] H. Mirahki, M. Moallem, M. Ebrahimi, and B. Fahimi, "Asymmetrical magnet shape optimization based on S-C mapping for torque profile mitigation in unidirectional application of SPMS machine," *IEEE Trans. Transp. Electrific.*, vol. 5, no. 3, pp. 630−637, Sep. 2019.

[16] K. Ramakrishnan, D. Zarko, A. Hanic, and G. Mastinu, "Improved method for field analysis of surface permanent magnet machines using Schwarz-Christoffel transformation," *IET Electr. Power App.*, vol. 11, no. 6, pp. 1067−1075, Jul. 2017.

[17] D. Cao, W. Zhao, T. Liu, and Y. Wang, "Magneto-electric coupling network model for reduction of PM eddy current loss in flux-switching permanent magnet machine," *IEEE Trans. Ind. Electron.*, vol. 69, no. 2, pp. 1189−1199, Feb. 2022.

[18] Zhou. Y and Wu. X, "Analytical calculation of magnetic field of bearingless flux-switching permanent-magnet machine based on doubly-salient relative permeance method," *IET Electr. Power App.*, vol. 14, no. 5, pp. 872−884, Feb. 2020.

[19] K. Boughrara, T. Lubin, and R. Ibtiouen, "General subdomain model for predicting magnetic field in internal and external rotor multiphase flux-switching machines topologies," *IEEE Trans. Magn.*, vol. 49, no. 10, pp. 5310−5325, Oct. 2013.

[20] S. Teymoori, A. Rahideh, H. Moayed-Jahromi, and M. Mardaneh, "2-D analytical magnetic field prediction for consequent-pole permanent magnet synchronous machines," *IEEE Trans. Magn.*, vol. 52, no. 6, Jun. 2016, Art no. 8202114.

[21] Q. Lu, B. Wu, Y. Yao, Y. Shen, and Q. Jiang, "Analytical model of permanent magnet linear synchronous machines considering end effect and slotting effect," *IEEE Trans. Energy Convers.*, vol. 35, no. 1, pp. 139−148, Mar. 2020.

[22] L. Wu, Z. Zhu, D. Staton, M. Popescu, and D. Hawkins, "An improved subdomain model for predicting magnetic field of surface-mounted permanent magnet machines accounting for tooth-tips," *IEEE Trans. Magn.*, vol. 47, no. 6, pp. 1693−1704, Jun. 2011.

[23] L. J. Wu, Z. Q. Zhu, D. Staton, M. Popescu, and D. Hawkins, "Subdomain model for predicting armature reaction field of surface-mounted permanent-magnet machines accounting for tooth-tips," *IEEE Trans. Magn.*, vol. 47, no. 4, pp. 812−822, Apr. 2011.

[24] L. J. Wu, Z. Q. Zhu, D. Staton, M. Popescu, and D. Hawkins, "Analytical prediction of electromagnetic performance of surface-mounted PM machines based on subdomain model accounting for tooth-tips," *IET Electr. Power App.*, vol. 5, no. 7, pp. 597−609, Aug. 2011.

Ying Fang received the B.Sc. degree in electrical engineering in 2020 from Jiangsu University, Zhenjiang, China. She is currently working toward the M. Sc. degree in control science and engineering at Jiangsu University.

Her current research interests include modeling and eddy current loss analysis for permanent magnet machine.

Jinghua Ji received the B.Sc., M.Sc., and Ph.D. degrees in electrical engineering from Jiangsu University, Zhenjiang, China, in 2000, 2003, and 2009 respectively.

Since 2000, she has been with the School of Electrical and Information Engineering, Jiangsu University, where she is currently a Professor in Electrical Engineering. From 2013 to 2014, she was a Visiting Scholar with the Department of Electronic and Electrical Engineering, University of Sheffield, Sheffield, U.K. Her areas of interest include motor design and electromagnetic field computation. She has authored and co-authored over 100 technical papers in these areas.

Wenxiang Zhao (M'08-SM'14) received the B.Sc. and M.Sc. degrees from Jiangsu University, Zhenjiang, China, in 1999 and 2003, respectively, and the Ph.D. degree from Southeast University, Nanjing, China, in 2010, all in electrical engineering. He has been with Jiangsu University since 2003, where he is currently a Professor with the School of Electrical Information Engineering.

From 2008 to 2009, he was a Research Assistant with the Department of Electrical and Electronic Engineering, University of Hong Kong, Hong Kong. From 2013 to 2014, he was a Visiting Professor with the Department of Electronic and Electrical Engineering, University of Sheffield, Sheffield, U.K. His current research interests include electric machine design, modeling, fault analysis, and intelligent control. He is the author or co-author of more than 150 papers published in various IEEE TRANSACTIONS.